RESEARCH PAPER

Nanoencapsulation of Coriandrum sativum Essential Oil in Solid Lipid Nanoparticles: Physicochemical Characterization, Antioxidant Activity and Short-Term Stability

Amir Firdaus bin Mokhtar[1], Samah Hamed Almurisi[2], Syed Mahmood[3], Rahul Pal[4], Fawaz Alheibshy[5], Nasrin E. Khalifa[5], Syed Haroon Khalid[1,6*], Khater AL-Japairai[1,7*]

[1]Department of Pharmaceutical Technology, Faculty of Pharmacy, Universiti Teknologi MARA, Puncak Alam 42300, Selangor, Malaysia

[2]Department of Pharmaceutical Technology, School of Pharmacy, IMU University, Kuala Lumpur 57000, Malaysia

[3]Department of Pharmaceutical Technology, Faculty of Pharmacy, Universiti Malaya, Kuala Lumpur 50603, Malaysia

[4]University Institute of Pharma Sciences (UIPS), Chandigarh University, Mohali, 140413, Punjab, India

[5]Department of Pharmaceutics, College of Pharmacy, University of Hail, 2240, Hail, Saudi Arabia

[6]Department of Pharmaceutics, Faculty of Pharmaceutical Sciences, Government College University Faisalabad, 38000, Faisalabad Pakistan

[7]Innovative Drug Development and Delivery Research Group (InDeeD), Faculty of Pharmacy, UiTM Cawangan Selangor, Bandar Puncak Alam, 42300, Selangor, Malaysia

***Corresponding authors:**

Khater AL-Japairai; khater@uitm.edu.my , ORCID: https://orcid.org/0000-0002-1426-9575

Syed Haroon Khalid; syedharoonkhalid@gcuf.edu.pk

Abstract

Coriander Essential Oil (CEO), a natural essential oil harvested from the seed of the coriander plant, is recognized for its biological activity, including antioxidant, anti-inflammatory and antimicrobial. However, its potential to be incorporated into pharmaceutical and cosmetic formulations is hindered by high volatility and chemical instability. To address these limitations, this study developed and evaluated solid lipid nanoparticles (SLNs) to improve CEO stability and biological activity. Five SLN formulations with varying ratios of glyceryl monostearate (solid lipid) to CEO (liquid lipid) were fabricated using high-speed homogenization combined with ultrasonication. The freshly prepared SLNs were characterized for particle size (PS), polydispersity index (PDI) and zeta potential (ZP) using a Zetasizer, while encapsulation efficiency (EE%) and loading capacity (LC%) were characterized using indirect UV spectrometry. GC-MS analysis identified linalool as the primary volatile constituent (56.20%), which correlated with the CEO's antioxidant profile. The prepared SLNs exhibited favorable physicochemical properties, with PS ranging from 80.60 ± 0.75 nm to 96.22 ± 0.89 nm, PDI between 0.217 ± 0.01 and 0.250 ± 0.01, and ZP values from -25.20 ± 2.74 mV to -37.40 ± 2.33 mV, confirming a monodisperse and electrostatically stable formulation. Remarkably, all formulations achieved an EE% above 97.79% and an LC% above 17.47%, with SLN 1 peaking at 99.56% ± 0.15 and 46.36% ± 0.29, respectively. The morphology of the optimized SLN 1 was uniform and spherical. In DPPH assays, SLN 1 exhibited moderate free radical-scavenging activity (62.11% ± 0.01). Furthermore, a 30-day short-term stability study at controlled room temperature (25 ± 2°C) and relative humidity (60%) confirmed that all physicochemical properties remained within acceptable ranges. Ultimately, these findings demonstrate that SLNs serve as an excellent protective delivery system for CEO, further enhancing both its antioxidant activity and storage stability for advanced pharmaceutical and cosmeceutical applications.

Keywords: Coriandrum sativum essential oil, solid lipid nanoparticles, high-speed homogenization, characterization, stability study, antioxidant activity.

How to cite this article: Amir Firdaus bin Mokhtar1 Samah Hamed Almurisi2 Syed Mahmood3 Rahul Pal4 Fawaz Alheibshy5 Nasrin E. Khalifa5 Syed Haroon Khalid16* Khater AL-Japairai17*. Nanoencapsulation of Coriandrum sativum Essential Oil in Solid Lipid Nanoparticles: Physicochemical Characterization, Antioxidant Activity and Short-Term Stability. Int J Drug Deliv Technol. 2026;16(90s):2177-2190. DOI: 10.25258/ijddt.16.90s.219.

Introduction

Coriandrum sativum, also known as the coriander plant, is an aromatic annual herb cultivated primarily for its essential oil-rich seeds, which are native to the region encompassing the Middle East, the East Mediterranean basin and the Caucasus Region, but is now cultivated worldwide, including China, Europe, India, Africa and various parts of Asia (1, 2). The genus *Coriandrum* is classified within the botanical family Apiaceae, formerly known as *Umbelliferae* (1). Within the genus, only two species are recognized, which are *C.sativum* and its wild species *C.tordylium* (3). *C.sativum* is the predominantly cultivated species with global commercial value for both its aromatic leaves and its nutrient-rich seeds (2). The Coriander Essential Oil (CEO) has been extensively studied for its diverse biological activities and health benefits, particularly regarding its traditional therapeutic uses as an antiemetic and carminative for gastrointestinal tract disorders to alleviate dyspepsia, flatulence and

diarrhea, as well as its potential antihyperlipidemic and antidiabetic activities in rat models (2, 3). The CEO is typically a colourless or pale yellow liquid that is synthesized and stored within specialized oil ducts known as vittae located throughout the vegetative and reproductive organs of the plant (4, 5). The CEO is comprised of a complex mixture of secondary metabolites, which function to facilitate plant survival against pathogens, environmental stressors and interaction with other organisms (6). The primary source of the essential oil is mostly extracted from the seeds by using either traditional techniques, such as hydrodistillation or modern techniques like microwave-assisted hydrodistillation (7). The phytochemical profile of CEO is generally dominated by terpenoid compounds (8). Despite that, the exact qualitative and quantitative distribution of the essential oil can vary significantly based on geographic origin, climatic variations and both biotic and abiotic influences (9, 10). The most notable terpenoid is linalool, which is responsible for exhibiting various biological activities such as anti-inflammatory, antimicrobial and antioxidant activities (2, 8).

Although the CEO possesses promising biological activities, the chemical instability of the CEO has become a major limiting factor to its biological activity (11). The CEO principal components, such as linalool, are volatile and degrade easily when exposed to environmental factors like heat, light and oxygen (11). Upon contact with environmental factors, the essential oils evaporate easily and undergo chemical reactions such as oxidation, isomerization or dehydrogenation, which further alter the biological activities over time. (12). Furthermore, exposure to elevated temperatures accelerates alterations in the essential oil's phytochemical profile, limiting its incorporation into stable pharmaceutical and cosmetic products (11). For instance, linalool is dehydrogenated into a mixture of inactive compounds, including ß-myrcene, cis-ocimene and trans-ocimene, when exposed to thermal degradation (13). Hence, the nanotechnology encapsulation method, such as liposomes, nanoemulsions and nanocapsules, has been studied to enhance the essential oil chemical stability by addressing those aforementioned limitations (14).

Among the available nanotechnology encapsulation methods, solid lipid nanoparticles (SLNs) offer a promising approach due to their small particle size, high loading capacity and ability to protect the active ingredients from environmental stressors (15, 16). Besides, the solid lipid matrix facilitates control of essential oil volatility by reducing the evaporation of their volatile constituents, thereby improving formulation stability (16). In terms of drug delivery ability, SLNs can enhance the water solubility, bioavailability and improve the intracellular permeability of the encapsulated materials (15, 17). Since this approach has already proven successful in previous research with other essential oils, such as *Origanum vulgare* and *Thymus vulgaris* essential oil-loaded SLNs (18), SLNs represent an ideal carrier system for encapsulating the CEO.

This study focused on developing and optimizing CEO-loaded SLNs by adjusting formulation parameters, particularly the concentrations of both the lipid matrix, which is glyceryl monostearate (GMS), and the active CEO. The formulated SLNs were evaluated based on their physical appearance, morphology, particle size, polydispersity index, zeta potential, encapsulation efficiency, loading capacity, DPPH assay for antioxidant activity and stability under temperature (25 ± 2°C) and relative humidity (60%). Ultimately, this research demonstrates that the composition adjustment of lipid nanocarriers could be a suitable strategy for enhancing both the chemical stability and biological activity of CEO.

1.0 Material and Methods

1.1 Materials

The pure CEO, utilized as the liquid lipid component, was imported from Russia and purchased through D'Naturel Official Store (Malaysia). The non-ionic surfactants, which were polyoxyethylene sorbitan monooleate 80 (Tween 80) and sorbitan monooleate (Span 80), were obtained from BRE Care Sdn, Bhd. (Malaysia) and R&M Chemicals (Malaysia), respectively. Glyceryl monostearate (GMS), which served as the solid lipid matrix, was procured from Chemiz (M) Sdn. Bhd. (Malaysia). All other solvents and reagents employed throughout this study were of analytical grade.

1.2 Gas chromatography coupled to a mass spectrometer (GC-MS)

The phytochemical profile of CEO was analyzed by using a GC-MS system (Agilent 7890A Gas Chromatography System coupled with Mass Spectrometry 5975 C, United States) that was equipped with an HP-5MS UI capillary column (5% diphenyl / 95% dimethylpolysiloxane, 30 m length x 0.25 mm internal diameter x 0.25 µm film thickness). For the analysis, a 10 µL syringe was used to inject a 1 µL sample of CEO, diluted with hexane at a 1:10 ratio. The sample was injected in split mode with a split ratio of 10:1, using helium as the carrier gas at a flow rate of 1 mL/min. The temperatures for the injector, transfer line interface and ion source were all maintained at 250°C. The GC oven settings commenced at an initial temperature of 50°C for 3 minutes, followed by an increment of 10°C/min to 180°C and 45°C/min to 280°C. The MS detection was performed in electron ionization (EI) mode at 70 eV, monitoring a scan range from 35 to 400 m/z. Data processing and evaluation were managed through the GC-MS Solution software package in conjunction with OpenChrom® (19).

1.3 Preparation of Coriandrum sativum essential oil-loaded SLNs.

Five formulations of CEO-loaded SLNs with varying solid lipid to essential oil ratios were formulated by using high-speed homogenization followed by ultrasonication techniques, as shown in Figure 1. Firstly, the lipid phase was prepared by melting glyceryl monostearate as a solid lipid matrix at 5-10°C above its melting point, which is at 70°C under gentle stirring. Next, the CEO and Span 80 surfactant were mixed into the molten solid lipid matrix under gentle stirring. The aqueous phase was prepared by heating the deionized water together with the Tween 80 surfactant under gentle stirring. The aqueous phase was heated to the same temperature as the lipid phase to avoid premature lipid solidification. The hot aqueous phase was added gradually and slowly into the hot lipid phase and was subjected to high-speed homogenization at 12,000 rpm for 15 minutes by using a D-Series Digital Benchtop Homogenizer (PRO Scientific Inc., Oxford, USA). Subsequently, the resulting emulsion was ultrasonicated for 5 minutes at 60% amplitude with a pulse time of 15 seconds to achieve a finer particle size by using Ultrasonic Processors 500W (Sigma-Aldrich, United Kingdom). The emulsion was cooled immediately in an ice bath to solidify the lipid phase and form solid lipid nanoparticles. Lastly, the freshly prepared formulations were stored at room temperature (20). The chemical composition of each of the five formulations of CEO-loaded SLNs is shown in Table 1.

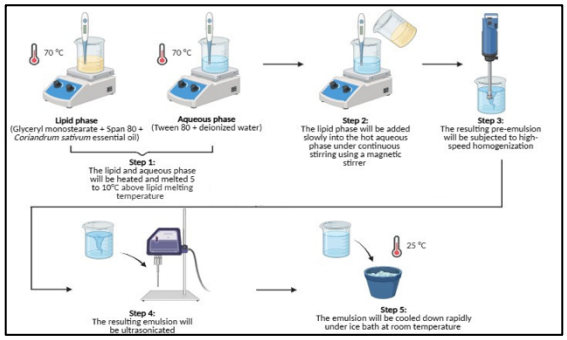


Figure 1. Schematic diagram of preparation of CEO-loaded SLNs

Table 1. Chemical composition of CEO-loaded SLNs.

Sample	Glyceryl Monostearate (w/w %)	*Coriandrum sativum* Essential Oil (w/w %)	Tween 80 (v/v%)	Span 80 (v/v%)	Deionized water (v/v %)	Solid Lipid to Essential Oil Ratio
SLN 1	1.0	1.0	0.4	0.4	17.2	50:50
SLN 2	1.2	0.8	0.4	0.4	17.2	60:40
SLN 3	1.4	0.6	0.4	0.4	17.2	70:30
SLN 4	1.5	0.5	0.4	0.4	17.2	75:25
SLN 5	1.6	0.4	0.4	0.4	17.2	80:20

1.4 Physicochemical Characterization of SLNs

1.4.1 Physical appearances

The physical appearances of CEO-loaded SLNs were evaluated routinely throughout the study via visual inspection. Each formulation was monitored for changes in colour and homogeneity, as well as signs of physical instability such as phase separation, visible aggregation, creaming, coalescence, flocculation and crystallization to detect potential stability problems (21).

1.4.2 Particle size (PS), polydispersity index (PDI) and zeta potential (ZP)

Particle size and polydispersity index values of the CEO-loaded SLNs were analyzed via the dynamic light scattering (DLS) method, while zeta potential values were determined via electrophoretic light scattering (ELS) method by using a Zetasizer Nano-ZS90 (Malvern Instruments Ltd., Worcestershire, UK). Before analysis, all samples were diluted in a 1:100 ratio with distilled water. The measurements of each parameter were conducted at a controlled temperature of 25 ± 2°C at specific intervals (t = 0 and t = 30). All analyses for each sample were performed in triplicate at room temperature (22).

1.4.3 Oil encapsulation efficiency (EE%)

The encapsulation efficiency (EE%) of CEO-loaded SLNs was evaluated through an indirect UV-Vis spectrophotometric method. Firstly, a 1000 µg/mL stock solution of pure CEO was prepared in 95% ethanol. The stock solution was sequentially diluted to yield a series of standard calibration solutions at concentrations of 10 µg/mL, 20 µg/mL, 30 µg/mL, 40 µg/mL, 50 µg/mL and 60 µg/mL. The absorbance values were measured at 226 nm using a Biobase BK-UV1000G UV-Vis spectrophotometer (BIOBASE Group, China) to generate a calibration curve. From this established standard curve, the following linear regression equation was derived:

$$y = 0.0159x + 0.0069,\ R^2 = 0.9992$$

Where x represents the concentration of the CEO µg/mL, y represents the measured absorbance at 226 nm. To quantify the unencapsulated (free) oil, 4 mL aliquots of each CEO-loaded SLNs formulation were subjected to ultracentrifugation at 25,000 rpm for 70 minutes at 4°C by using an Optima MAX-XP Tabletop Ultracentrifuge (Beckman Coulter Life Sciences Inc., United States). This process separated the encapsulated oil pellet from the supernatant containing the free oil. The supernatant was

carefully isolated by using a glass pipette to avoid disturbing the pellet. Subsequently, the supernatant was diluted in a 1:50 ratio with ethanol to ensure the absorbance fell within the linear range of the calibration curve. The absorbance of each supernatant sample was measured at 226 nm in triplicate. The concentration of free CEO was calculated by using the previously established linear regression equation (18). The encapsulation efficiency (EE%) was calculated by using the following formula:

$$EE\ (\%) = = \frac{W_{total\ essential\ oil} - W_{free\ essential\ oil}}{W_{total\ essential\ oil}} \times 100$$

Where: $W_{total\ essential\ oil}$ represents the initial amount of CEO added to the SLNs formulation. $W_{free\ essential\ oil}$ represents the amount of free CEO found in the supernatant (23).

1.4.4 Loading capacity (LC%)

The loading capacity (LC%) of the CEO-loaded SLNs was determined following a similar indirect UV-Vis spectrophotometer quantification and ultracentrifugation method used for encapsulation efficiency. After determining the concentration of free copaiba oil via the established standard calibration curve, the loading capacity was calculated by using the following formula:

$$LC\ (\%) = \frac{W_{total\ essential\ oil} - W_{free\ essential\ oil}}{W_{total\ essential\ oil} - W_{free\ essential\ oil} + W_{total\ lipid}} \times 100$$

Where: $W_{total\ essential\ oil}$ represents the initial amount of CEO added to the SLNs formulation. $W_{free\ essential\ oil}$ represents the amount of free CEO found in the supernatant. $W_{total\ lipid}$ represents the amount of lipid in the SLNs formulation (23).

1.4.5 Morphology using Scanning Electron Microscope (SEM)

The structural morphology of an optimized SLN 1 formulation was evaluated using a FEI Quanta 450 FEG Scanning Electron Microscope (Thermo Fisher Scientific, Netherlands). A droplet of the sample was placed onto a glass coverslip and allowed to dry. The dried specimen was then coated with a thin layer of platinum to enhance the conductivity. The SEM micrograph imaging was performed at an accelerating voltage of 5.0 kV with a magnification of 20,000× (15).

1.5 DPPH radical scavenging activity (RSA)

The antioxidant activity of the CEO-loaded SLNs was evaluated by using the stable 2,2-diphenyl-1-picrylhydrazyl (DPPH) radical scavenging assay based on the classic method described by Blois. This method measured the electron-donating capacity of the CEO-loaded SLNs, which was quantified by monitoring the colorimetric bleaching of the purple DPPH to a yellow solution (24). To assess the antioxidant activity, a 0.5 mL aliquot of each sample preparation, including the test nanoparticle formulation of SLN1, blank formulation of SLN1 without CEO and 50 µg/ml ascorbic acid as a positive control, was treated with a negative control of 1.0 mL of 0.1 mM ethanolic solution of DPPH. The reaction mixtures were agitated vigorously and incubated in the dark at room temperature (25 ± 2°C) for 30 minutes. Following incubation, the absorbance (A) of each solution was recorded at 517 nm against an ethanol blank by using a Biobase BK-UV1000G UV-Vis spectrophotometer (BIOBASE Group, China). The radical scavenging activity was expressed as the percentage of DPPH discoloration and calculated via the following equation:

$$RSA\ (\%) = \frac{A_{control} - A_{sample}}{A_{control}} \times 100$$

Where: $A_{control}$ represents the absorbance of the blank formulation containing DPPH dissolved in ethanol, A_{sample} represents the absorbance of the tested solution, including the test sample, or standard (25).

1.6 Stability study

A short-term stability study was conducted on the CEO-loaded SLNs over one month. The formulations were stored under controlled conditions at a temperature of 25 ± 2°C and a relative humidity of 60%. The physical and chemical stability of the SLNs was monitored at regular and fixed intervals of Day 0 and Day 30 based on variations in visual appearance, particle size, polydispersity index, zeta potential, encapsulation efficiency (EE%) and loading capacity (LC%) (26).

1.7 Statistical Analysis

Statistical analysis was conducted using the Microsoft Excel tool. A one-way analysis of variance (ANOVA) was executed to evaluate the impact of different GMS-to-CEO ratios on SLNs characteristics such as particle size, PDI and zeta potential during the optimization phase. For the stability study, a paired t-test was utilized to statistically compare the physicochemical properties of SLNs between baseline measurement (Day 0) and final measurement (Day 30) under controlled room temperature (25 ± 2°C) and relative humidity (60%). For all statistical operations, significance was established at $p < 0.05$.

2.0 Results and Discussions

2.1 GC-MS analysis of Coriandrum sativum essential oil

The chemical composition of the CEO was successfully elucidated by using GC-MS. Chromatographic analysis, as shown in Figure 2, revealed 10 volatile constituents that varied in both retention time and peak areas. This finding is consistent with the typical phytochemical fingerprint of the essential oil produced by *Coriandrum sativum* species as reported in several GC-MS analysis studies (27). The chemical constituent profile, along with individual retention times, relative percentages of peak areas, chemical

classifications, and characteristic mass-to-charge ratios (m/z), is systematically tabulated in Table 2.

The chromatographic analysis revealed that the CEO is overwhelmingly dominated by monoterpene and its derivatives, which account for the vast majority of the total volatile constituent fraction. Notably, the monoterpene alcohol linalool was identified as the major principal constituent by exhibiting a significant relative peak area of 56.20% at a retention time of 12.076 minutes. However, the aliphatic tertiary alcohol structure of linalool renders its molecular ion (m/z 154) unstable during ionization. Consequently, the m/z 154 peak is typically weak or absent in standard electron ionization (EI) spectra (28). Hence, the spectrum is dominated by stable fragment ions, particularly the base peak at m/z 71, followed by prominent signals at m/z 93 and m/z 55, as shown in Figure 3. This observation aligns with earlier studies that identify linalool as the predominant monoterpene in the essential oil secreted by *Coriandrum sativum* species (29, 30).

The CEO's therapeutic potential is largely attributed to this compound, which possesses well-documented anti-inflammatory, antimicrobial and antioxidant effects (2). Following linalool, other prominent monoterpene hydrocarbons and ketones were also detected in low abundance. These include α-pinene (4.91% at 7.221 min), camphor (4.50% at 13.218 min), isomeric pairs of cymene, particularly p-cymene and o-cymene (2.77% at 9.719 min) and γ-terpinene (2.54% at 10.704 min). Besides, the inclusion of trace constituents, including geranyl acetate (2.48% at 19.693 min), D-limonene (2.05% at 9.834 min) and Camphene (0.88% at 7.605 min) further exemplifies the extensive chemical complexity of the CEO (10). Despite their lower abundance, these compounds may actively contribute to the CEO's collective biological activity through synergistic mechanisms with major constituents to enhance the overall therapeutic efficacy of CEO (2, 10).

A critical evaluation of the chromatographic analysis revealed a specific co-elution phenomenon that arises from structural similarities among certain isomeric monoterpenes. The isomeric pairs of cymene, which are p-cymene and o-cymene, were observed to co-elute precisely at a retention time of 9.719 minutes with a peak area of 2.77%. This co-elution is a consequence of the chemical constituents possessing identical boiling points and similar thermodynamic affinities for the non-polar stationary phase utilized in the capillary GC column (31).

Furthermore, variations in compound abundance can arise due to several factors, such as geographical origin, climatic variations, extraction methods and biotic to abiotic factors (9, 10). Nevertheless, the core phytochemical profile perfectly matches the pure CEO as reported in several literature sources, thereby verifying the purity and authenticity of the CEO used in this study (27, 29, 30). Therefore, the presence of volatile linalool molecules in high abundance, with the presence of minor chemical constituents, highlights the chemical viability of the CEO for both therapeutic applications and integration into SLNs (11).

Table 2. Identified chemical constituents of the CEO by using GC-MS anaylsis.

Name of Compound	Retention Time (min)	Peak Area (%)	Class of Compound	m/z
Linalool	12.076	56.20	Monoterpene alcohol	73/93/55
α-pinene	7.221	4.91	Monoterpene hydrocarbon	93/91/92
Camphor	13.218	4.50	Monoterpene ketone	95/81/108
Methylcyclopentane	2.282	4.25	Cycloalkane	56/69/55
p-cymene	9.719	2.77	Monoterpene hydrocarbon	119/134/91
o-cymene	9.719	2.77	Monoterpene hydrocarbon	119/134/91
γ-terpinene	10.704	2.54	Monoterpene hydrocarbon	93/91/136
Geranyl acetate	19.693	2.48	Monoterpene ester	69/68/93
D-limonene	9.834	2.05	Monoterpene hydrocarbon	68/93/67
Camphene	7.605	0.88	Monoterpene hydrocarbon	93/121/79

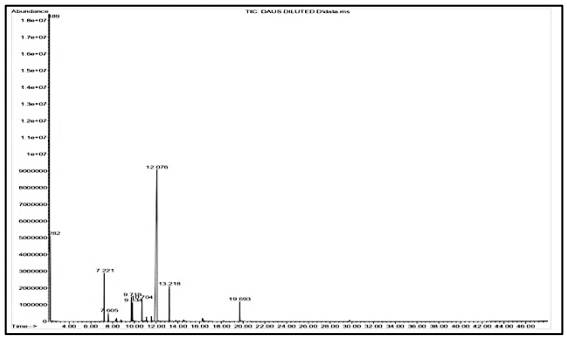


Figure 2. GC-MS spectra of the CEO.

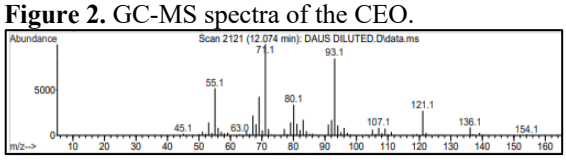


Figure 3. GC-MS analysis for linalool.

2.2 Characterization of CEO-loaded SLNs

2.2.1 Particle size

The five formulations that vary in their GMS-to-CEO ratios have exhibited distinct differences in average particle size (PS), polydispersity index (PDI), and zeta potential (ZP). A higher proportion of liquid lipid (CEO) directly correlated with an increase in PS, as detailed in Table 3. The particle size analysis for the CEO-loaded SLNs is visually represented in Figure 4. SLN 1 exhibits the minimum mean particle size of 80.60 ± 0.75 nm with an equal GMS-to-CEO ratio of 50:50. An incremental shift in the ratio has progressively increased the SLN average PS, ascending through 84.63 ± 0.41 nm (SLN 2), 92.29 ± 0.44 nm (SLN 3) to 94.81 ± 0.33 nm (SLN 4). SLN 5 has recorded the maximum average PS at 96.22 ± 0.89 nm with the highest GMS-to-CEO ratio of 80:20. Comprehensive statistical analysis through One-way Analysis of Variance (ANOVA) revealed a statistically significant difference in PS across the different formulation ratios ($p = 7.34 \times 10^{-11}$). Because the p-value is profoundly lower than the standard significance threshold ($\alpha = 0.05$), it firmly establishes that the variations in the lipid matrix composition exert a statistically significant effect on the final average PS of the SLNs.

This observation is consistent with the established principle that an increase in solid lipid (GMS) concentration and a decrease in the liquid lipid (CEO) concentration lead to a proportional increase in the average PS of the nanoparticles (32). Higher GMS concentration increases the colloidal dispersion viscosity that impedes the emulsification process and drives the formation of larger SLNs (32). Conversely, the incorporation of the CEO reduces the system viscosity and consequently contributes to the PS reduction (33). Furthermore, increasing the CEO concentration within the lipid phase decreases the viscosity of the molten lipid during the homogenization and ultrasonication process, thereby producing smaller nanoparticle sizes. Consistently, similar findings with other essential oil-loaded SLNs have reported that higher concentrations of solid lipid increase the average PS, driven by a greater tendency for the nanoparticles to coalesce at high solid lipid concentrations (34). Other findings suggest that increasing lipid concentration increases the PS due to density differentials between the internal and external phases (26). Moreover, despite PS variations across all formulations, all formulations maintained PS in the range of 50 nm to 300 nm, which is generally recognized as an established indicator of an optimized SLN with excellent physical stability and enhanced biological activity (15).

Table 3. The particle size, PDI and zeta potential of CEO-loaded SLNs with different solid-to-liquid lipid ratios at Day 0 (mean ± SD, N = 3).

Sample	GMS-to-CEO ratio	Particle size (nm)	PDI	Zeta potential (mV)
SLN 1	50:50	80.60 ± 0.75	0.218 ± 0.01	-34.0 ± 0.98
SLN 2	60:40	84.63 ± 0.41	0.217 ± 0.01	-25.2 ± 2.74
SLN 3	70:30	92.29 ± 0.44	0.225 ± 0.01	-31.9 ± 0.70
SLN 4	75:25	94.81 ± 0.33	0.249 ± 0.01	-31.9 ± 2.02
SLN 5	80:20	96.22 ± 0.89	0.250 ± 0.01	-37.4 ± 2.33

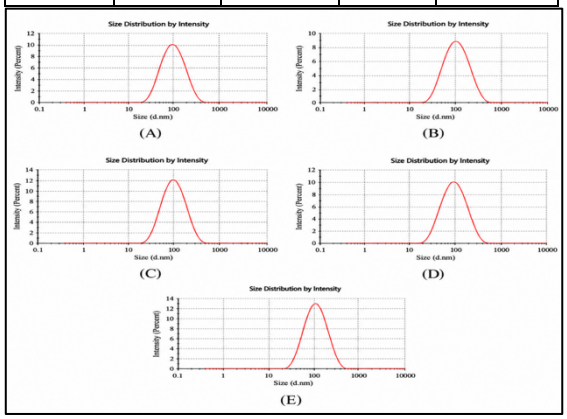


Figure 4. Particle size distribution of CEO-loaded SLNs with (A) SLN1, (B) SLN2, (C) SLN3, (D) SLN4 and (E) SLN5.

2.2.2 Polydispersity index (PDI)

The polydispersity index (PDI) serves as an essential indicator of colloidal dispersion homogeneity that reflects the uniformity of the particle size distribution (35). Within this parameter, the values below 0.3 define a monodisperse and narrow size distribution, whereas values exceeding 0.3 denote a polydisperse and broad particle size distribution (36). Low PDI value (<0.3) is associated with greater colloidal stability over time, which indicates that the

particles do not aggregate and remain stable during storage (37). However, a high PDI value (>0.3) is a marker of formulation instability, aggregation and sedimentation (15). Hence, PDI is an important parameter to assess the quality of CEO-loaded SLNs. The experimental data display a distinct and non-linear upward trend in PDI values as the proportion of the GMS increases relative to the CEO. The PDI remains remarkably low, ranging from 0.217 ± 0.01 (SLN 2) to 0.225 ± 0.01 (SLN 3). This indicates a stable, monodisperse system where the liquid lipid (CEO) is successfully integrated into the solid lipid core (GMS). A sharp increase in PDI is observed, shifting from 0.249 ± 0.01 (SLN 4) to 0.250 ± 0.01 (SLN 5), respectively. While the PDI of these formulations still falls within an acceptable range (<0.3), the higher values denote an increase in particle size polydispersity. Nonetheless, all recorded PDI values are less than 0.3, indicating that all five formulations maintain an acceptable, narrow and monodisperse distribution within the CEO-loaded SLNs system. The statistical analysis revealed a statistically significant difference in the PDI value across the five formulations ($p = 8.66 \times 10^{-5}$). Since the p-value falls below the standard significance criteria ($\alpha = 0.05$), it confirms that altering the GMS-to-CEO ratios exerts a statistically significant impact on the monodispersity of the SLNs system.

An upward trend in PDI was observed as the solid lipid concentration increased from SLN 1 to SLN 5. This pattern aligns with findings published by Mura et al. (38), who highlighted that higher concentrations of solid lipids, while keeping surfactant concentrations constant can significantly alter the PDI due to relative decrease in the surfactant-to-lipid ratio. The increase in PDI may be attributed to nanoparticles fusion, a process where individual nanoparticles merge into larger aggregates and consequently increase the overall particle size distribution (35).

2.2.3 Zeta potential (ZP)

Zeta potential (ZP) measures the surface charge magnitude of nanoparticles in aqueous media, reflecting their electrostatic properties and stability (39). For electrostatically stable SLNs, a ZP value greater than ± 30 mV is optimal to prevent particle aggregation due to strong repulsive forces (39). The data show that the ZP values for CEO-loaded SLNs ranged from -25.2 ± 2.74 mV (SLN 2) to -37.4 ± 2.33 mV (SLN 5) and the visual representation of ZP data is displayed in Table 3 and Figure 5, respectively. The negative ZP observed in all five formulations can be attributed to the particular components of the SLN matrix. Specifically, the presence of ionized carboxyl groups ($-COO^-$) within the GMS solid lipid. generates electrostatic repulsion that effectively prevents potential nanoparticle aggregation (40). Furthermore, the inclusion of Tween 80 as a hydrophilic and non-ionic surfactant provides steric stabilization against nanoparticle aggregation while simultaneously enhancing the formulation's thermal, mechanical and freeze-thaw stability (40). Besides, incorporation with lipophilic Span 80 surfactants further provides a stable interfacial film and increases emulsification process performance (41). The ZP value for all SLNs formulation are greater than ± 30 mV, indicating a strong electrostatic stability, except for SLN 2 with a less negative value (< ± 30 mV). Nonetheless, the ZP value for all formulations falls within the acceptable range. The statistical analysis by using ANOVA revealed a statistically significant difference across the formulation ($p = 2.35 \times 10^{-4}$), which is less than the established criteria ($\alpha = 0.05$). This p-value demonstrates that variations in the GMS-to-CEO ratio significantly influence the ZP of SLNs. The increasing trend of ZP across the five formulations corresponds with observations by Soleimani et al. (42), where the SLNs' surface charge initially became less negative at a lower ratio (SLN 1) but became increasingly negative as the ratio was further increased (SLN 5). This phenomenon can be attributed to the high concentration of solid lipids that affects the charge distribution and surfactant alignment at the interfacial film of the SLNs.

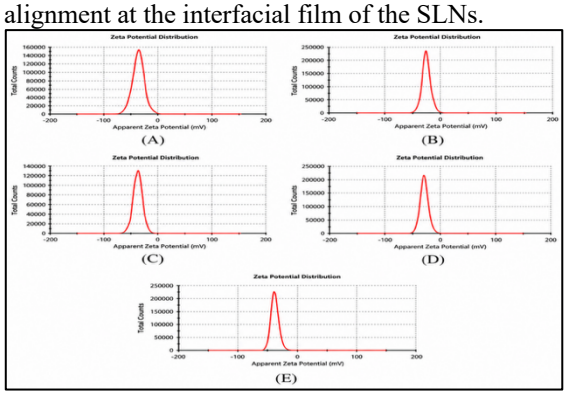


Figure 5. Zeta potential distribution of CEO-loaded SLNs with (A) SLN1, (B) SLN2, (C) SLN3, (D) SLN4 and (E) SLN5.

2.2.4 Encapsulation Efficiency (EE%)

The EE% and LC% values of CEO-loaded SLNs prepared at varying GMS-to-CEO ratios are presented in Table 4. EE% parameter measures the capability of SLNs to effectively entrap and retain active ingredients, which is the CEO, within the SLNs' core matrix (39). Achieving a high EE% value is important to secure an adequate therapeutic payload and active ingredient wastage reduction throughout the production process (43). Ultimately, the EE% is dictated by specific lipid composition. The solubility of the essential oil within the solid lipid matrix and the SLNs production technique employed (44).

The experimental data reveals a linear downward trend with the inversely proportional relationship between the GMS-to-CEO ratio. SLN 1 contain the highest proportion of CEO achieved the highest EE%

(99.56%). As the GMS ratio systematically increases, a gradual and steady decline is observed in EE% from SLN 2 (99.22%) to SLN 4 (98.31%). SLN 5 (97.79%) with the highest GMS ratio exhibits the lowest EE% among the formulations. Despite that, all of the formulations remained within the efficient range, which is more than 70% (11). In addition, the previous studies conducted on other essential oils show a similar trend, where an increase in solid lipid concentration leads to a decrease in EE% (18, 34). This phenomenon can be attributed to the crystallization process of the highly ordered solid lipid into a crystalline lattice that leads to the expulsion of the essential oil into the surrounding water phase, producing low EE% as the solid lipid ratio increases (45, 46).

2.2.5 Loading Capacity (LC%)

LC% parameters define the mass ratio of the encapsulated CEO to the total weight of the nanoparticle, indicating the amount of CEO that can be effectively held within the nanoparticle (39). The LC% exhibited a downward trend as the solid lipid ratio increased, as presented in Table 4. The LC% values range from 46.36% (SLN 1) to 17.51% (SLN 5). This can be due to the crystalline solids, which tend to expel the active ingredient by forming a more ordered crystal lattice, leading to lower LC% (39).

Table 4. The encapsulation efficiency and loading capacity of CEO-loaded SLNs with different solid-to-liquid lipid ratios at Day 0 (mean ± SD, N = 3).

Sample	Encapsulation Efficiency (EE%)	Loading Capacity (LC%)
SLN 1	99.56 ± 0.15	46.36 ± 0.29
SLN 2	99.22 ± 0.17	36.47 ± 0.20
SLN 3	98.86 ± 0.24	26.89 ± 0.31
SLN 4	98.31 ± 0.20	22.15 ± 0.18
SLN 5	97.79 ± 0.19	17.51 ± 0.25

2.2.6 Scanning electron microscopy (SEM)

The surface morphology of the optimized SLN 1 formulation was examined using SEM as shown in Figure 6. The micrograph showed that the vesicles appeared uniform, with a predominance of spherical shape and an overall acceptable nanoparticle size distribution of SLN.

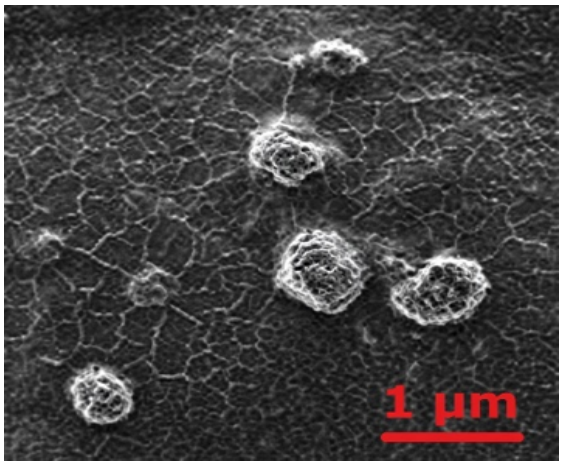


Figure 6. Scanning electron micrograph of the optimized CEO-loaded SLN 1 at 20,000X magnification.

2.3 Antioxidant activity

For this assay, SLN 1 was selected as the test sample because it has the best physicochemical characteristics among the formulations. To evaluate antioxidant potential, the DPPH radical-scavenging assay was employed, with all samples evaluated at a fixed concentration of 50 µg/mL. In this study, the CEO-loaded SLNs 1 demonstrated a moderate antioxidant activity with a radical scavenging activity of 62.11% ± 0.31, as shown in Table 5. The ascorbic acid standard served as the positive control and yielded the antioxidant effect at 96.58% ± 0.46 of radical scavenging activity. The CEO is rich in monoterpenes particularly linalool, which are known for their ability to interact with and stabilize free radicals (2, 10). This moderate antioxidant performance is consistent with prior research, which reported a range of approximately 50% to 67% antioxidant activity of the CEO using the radical scavenging assay (10, 47, 48). This antioxidant performance in this study can be primarily attributed to the high abundance of linalool and potential synergistic interactions with minor volatile components present within the essential oil phytochemical profile, as shown in the GC-MS analysis (10). The experimental data suggest that the SLN successfully preserved the antioxidant activity of these volatile components. Hence, this evidence supports the potential of CEO-loaded SLNs as an effective antioxidant delivery system.

Table 5. Antioxidant activity (radical scavenging activity % of DPPH) of the standard and test sample (mean ± SD, N = 3).

Sample	Concentration (µg/ml)	Radical scavenging activity (%)
Standard (ascorbic acid)	50	96.58% ± 0.46
Test (SLN 1)	50	62.11% ± 0.31

2.4 Stability Study

All formulations (SLN 1 – SLN 5) were selected for the stability study due to their optimal initial PS, PDI, ZP, %EE and %LC parameters. Each parameter of the developed SLN formulations was monitored over a 30-day storage period under controlled room temperature (25 ± 2°C) and relative humidity (60%), as shown in Table 6. A comparison between baseline measurement (Day 0) and final measurement (Day 30) revealed negligible shifts in PS and PDI, indicating that the SLNs resisted coalescence or aggregation issues. This structural integrity is supported by the sustained ZP values that maintained sufficient electrostatic repulsion to prevent particle clustering. Furthermore, the absence of a significant drop in %EE and %LC confirms that the solid lipid matrix effectively retained the volatile CEO. These results demonstrate that the formulations possess excellent short-term physical and chemical stability.

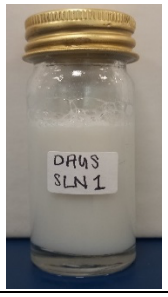
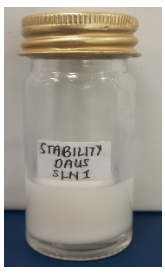
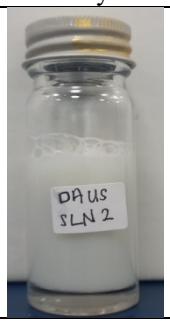
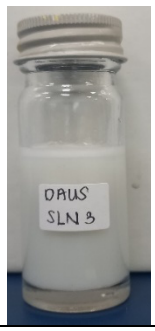
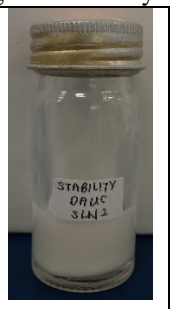
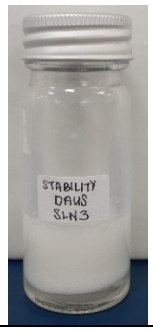
Table 6. The particle size, PDI, zeta potential, encapsulation efficiency and loading capacity of CEO-loaded SLNs with different solid-to-liquid lipid ratios at Day 30 (mean ± SD, N = 3).

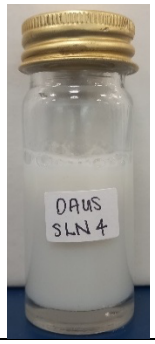
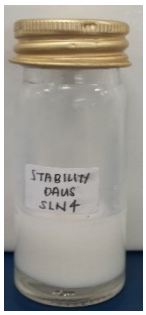
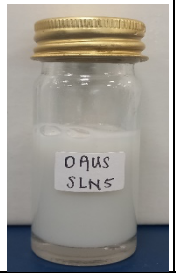
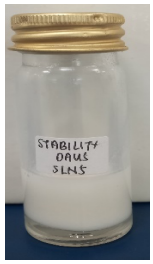
Sample	GMS-to-CEO ratio	Particle size (nm)	PDI	Zeta potential (mV)	Encapsulation Efficiency (EE%)	Loading Capacity (LC%)
SLN 1	50:50	82.83 ± 0.62	0.230 ± 0.01	-32.4 ± 0.55	99.41 ± 0.17	46.32 ± 0.23
SLN 2	60:40	89.35 ± 2.77	0.231 ± 0.01	-21.8 ± 0.20	99.04 ± 0.22	36.43 ± 0.30
SLN 3	70:30	93.67 ± 0.53	0.237 ± 0.01	-30.1 ± 0.66	98.65 ± 0.29	26.85 ± 0.26
SLN 4	75:25	95.26 ± 0.26	0.253 ± 0.01	-30.3 ± 0.62	98.08 ± 0.16	22.10 ± 0.19
SLN 5	80:20	99.30 ± 0.53	0.260 ± 0.01	-33.8 ± 0.35	97.53 ± 0.20	17.47 ± 0.24

2.4.1 Physical appearance

Visual evaluation of the CEO-loaded SLN formulations was conducted on Day 0 and Day 30 under controlled room temperature (25 ± 2°C) and relative humidity (60%). At baseline (Day 0), all SLN samples appeared as uniform, milky-white to off-white, opaque colloidal dispersions despite varying GMS-to-CEO ratios. Over the 30-day storage monitoring period, Table 7 illustrates that the formulations exhibited excellent stability, with no detectable signs of phase separation, creaming, sedimentation, flocculation or crystallization (49). The formulations preserved the original colour, homogeneity and minimal oil leakage, further confirming that all developed SLNs maintained outstanding physical stability throughout the study.

Table 7. The physical appearance of all CEO-loaded SLN formulations on Day 0 & Day 30.

Sample	GMS-to-CEO ratio	Day 0	Day 30
SLN 1	50:50		
SLN 2	60:40		
SLN 3	70:30	 	 

SLN 4	75:25		
SLN 5	80:20		

2.4.2 Effect of storage time on characterization parameters

2.4.2.1 Particle size (PS)

The mean PS after a 30-day storage period ranged from 82.83 ± 0.62 nm (SLN 1) to 99.30 ± 0.53 nm (SLN 5) at controlled room temperature (25 ± 2°C) and relative humidity (60%) as shown in Table 6. A gradual increase in mean PS were observed across all formulations after 30 days of storage. However, paired t-test analysis as displayed in table 9 showed this upward trend was not statistically significant ($p > 0.05$). The increase in mean PS can be attributed to several factors such as GMS crystallization and Ostwald ripening that may impact the PS over time (50, 51). Despite that, all formulations exhibit PS within the ideal range, which is below 300 nm. Besides, previous studies conducted by Rahman et al (52) and Chantaburanan et al. (53) had shown minimal variation in PS when stored at room temperature, further supporting the stability observed in this study. Overall, the results confirm that all formulations maintained acceptable physical stability regarding particle size over 30 days, further indicating that room temperature is ideal for CEO-loaded SLNs storage.

2.4.2.2 Polydispersity index (PDI)

The PDI of CEO-loaded SLNs was evaluated for PS distribution after 30 days of storage at controlled room temperature (25 ± 2°C) and relative humidity (60%) as shown in Table 6 as detailed in Table 6. PDI values ranged from 0.230 ± 0.01 (SLN 1) to 0.260 ± 0.01 (SLN 5). Statistical analysis demonstrated that the PDI values for all five formulations showed no significant difference ($p > 0.05$) between Day 0 and Day 30 as presented in Table 9. This lack of statistical significance indicates that the uniformity and monodispersity of the SLNs were successfully maintained throughout the storage period. Moreover, all formulations remained within the acceptable size distribution because the PDI value is less than 0.5, indicating that the SLNs were stable during storage. These findings correspond with the data reported by Oboh et al. (54), where properly stabilized SLNs containing non-ionic surfactant exhibited minimal fluctuations over time. Ultimately, the results demonstrate that all CEO-loaded SLNs maintained excellent homogeneity over a 30-day storage period, with the best results observed in formulations using an optimized lipid ratio.

2.4.2.3 Zeta potential (ZP)

The ZP value for all CEO-loaded SLNs was in between the range of -21.8 ± 0.20 (SLN 2) and -33.8 ± 0.35 (SLN 5) as presented in Table 6 following 30-day storage period at controlled room temperature (25 ± 2°C) and relative humidity (60%), suggesting that the electrostatic stability was successfully maintained. The ZP values across all formulations fall within the desired range to preserve the colloidal dispersion stability. Statistical analysis, as displayed in Table 9, revealed that the changes in zeta potential values were not statistically significant ($p > 0.05$) for all tested formulations after 30 days of storage. Normally, a ZP value higher than 30 mV is accepted as appropriate, but the low ZP value seen in SLN 2 can be due to the attraction force between the particles being higher than the repulsion force, leading to flocculation or particle aggregation (55). This slight reduction in ZP value can be explained by surfactant redistribution or leakage from the SLNs over time, causing instability (56). These observations closely mirror the trend reported by Carvalho et al. (57) and Oboh et al (54), who both noted that while ZP values may experience minor variations during storage, they ultimately remain within acceptable baselines for stability. Overall, the results suggest that all CEO-loaded SLNs maintained an adequate electrostatic stability over a 30-day storage period.

2.4.2.4 Encapsulation efficiency (EE%)

The EE% of CEO-loaded SLNs remained exceptionally high and consistent after a 30-day storage period at controlled room temperature (25 ± 2°C) and relative humidity (60%). The EE% values varied marginally between 99.41% (SLN 1) and 97.53% (SLN 2) as summarized in Table 6, demonstrating negligible leakage of encapsulated CEO over storage period. The minor decrease in EE% observed in all SLNs can be attributed to lipid matrix relaxation or outward diffusion of weakly adsorbed CEO from the SLNs surface that frequently occur during storage. These outcomes strongly corroborate previous study on essential oil-loaded lipid nanocarriers, that document a high EE% with minimal loss over prolonged storage as similarly reported by Yu et al (58)., who noted that the

expulsion of essential oil can be due to the formation of more ordered lipid crystals. However, in a similar study, a significant drop in EE% was explained by a significant polymorphic transformation of the solid lipid crystal that occurred during storage (58). Conversely, Jamous et al. also reported a significant drop in EE% in their study at similar storage conditions, but this is due to inadequate surfactant coverage at elevated lipid concentrations (59). Nonetheless, the exceptionally high EE% maintained across all formulations after 30 days confirms the excellent structural integrity of the SLNs for long-term essential oil encapsulations.

2.4.2.5 Loading capacity (LC%)

The LC% for all five formulations remained remarkably stable by exhibiting only marginal and negligible reduction over the 30-day storage period at controlled room temperature (25 ± 2°C) and relative humidity (60%). The LC% ranges from 46.32% (SLN 1) to 17.51% (SLN 2). This issue can be attributed to a polymorphic transformation that converted the spherical α-subcell droplets into asymmetric and platelet-shaped β-subcell crystals that increase the crystalline ordering and compactness of the lipid matrix, which reduces the internal LC% of the SLNs and forces the expulsion of the encapsulated CEO (50, 60). Furthermore, as the GMS concentrations increase across the formulation, the downward trend in LC% can also be attributed to the increase in solid lipid ratios that is most likely to diminish the relative quantity of CEO that can be accommodated per unit weight of the GMS matrix. Despite that, SLN 1 can be considered to have the best performance for drug-loading capacity due to the ideal balance between EE% and LC% after 30 days of storage.

Table 8. Results of ANOVA analysis for all dependent variables of CEO-loaded SLNs formulations. P-values represent one-way ANOVA results comparing GMS-to-CEO ratio to each of the parameter. P < 0.05 indicates statistical significance.

Dependent Variables	p value	p value interpretation
PS	7.34×10^{-11}	Statistically significant
PDI	8.66×10^{-5}	Statistically significant
ZP	2.35×10^{-4}	Statistically significant

Table 9. Results of paired t-test analysis of short-term stability study evaluation of CEO-loaded SLNs. P-values represent paired t-test results comparing Day 0 and Day 30 for each parameter. P < 0.05 indicates statistical significance.

Sample	GMS-to-CEO ratio	Particle size (nm)	PDI	Zeta potential (mV)
SLN 1	50:50	p = 0.10 Not significant	p = 0.12 Not significant	p = 0.06 Not significant
SLN 2	60:40	p = 0.07 Not significant	p = 0.14 Not significant	p = 0.15 Not significant
SLN 3	70:30	p = 0.06 Not significant	p = 0.78 Not significant	p = 0.08 Not significant
SLN 4	75:25	p = 0.25 Not significant	p = 0.17 Not significant	p = 0.19 Not significant
SLN 5	80:20	p = 0.05 Not significant	p = 0.09 Not significant	p = 0.14 Not significant

2.5 Statistical analysis

All experimental measurements for CEO-loaded SLNs were performed in triplicate and are expressed as mean ± SD, N = 3. In this study, the impact of the independent variable (GMS-to-CEO ratio) on the dependent variables (PS, PDI, ZP, %EE, and %LC) of CEO-loaded SLNs was evaluated using one-way ANOVA, and the results are presented in Table 8. The stability comparison of CEO-loaded SLNs in the short-term stability study was conducted by using a paired t-test between Day 0 and Day 30 at controlled room temperature (25 ± 2°C) and relative humidity (60%). The results are systematically tabulated in Table 9 for each of the parameters before and after the short-term stability study.

3.0 Conclusion

In conclusion, CEO-loaded SLNs with GMS-to-CEO variations were successfully fabricated through high-speed homogenization combined with ultrasonication. All five developed formulations demonstrated favorable physicochemical properties, with PS spanning from 80.60 ± 0.75 nm to 96.22 ± 0.89 nm, PDI between 0.217 ± 0.01 and 0.250 ± 0.01, ZP values ranging from -25.20 ± 2.74 mV to -37.40 ± 2.33 mV, EE% reaching 97.79% ± 0.19 to 99.56% ± 0.15 and loading capacity from 17.51% ± 0.25 to 46.36% ± 0.29. Moreover, all SLN formulations exhibited good short-term stability with minimal variations in each characterization parameter and physical appearance after 30 days of storage. Based on these attributes, SLN 1 was chosen for antioxidant evaluation, where it exhibited a moderate radical scavenging activity of 62.11% ± 0.31. Hence, it suggests that the antioxidant potential of the CEO-loaded SLNs may be effectively preserved within the SLNs. Moreover, the SEM micrograph showed that the optimized SLN 1

exhibited a uniform and acceptable distribution of SLNs. Collectively, these findings underscore the potential of SLNs as a promising carrier system that is capable of enhancing the stability and biological activity of the CEO while addressing its limitations in pharmaceutical and cosmetic formulations.

Acknowledgement

The authors gratefully acknowledge the Faculty of Pharmacy, Universiti Teknologi MARA (UiTM) and Department of Pharmaceutical Technology for the facilities and technical assistance provided in the Biopharmaceutical Lab throughout this study.

Conflicts of Interests

The authors declare that there are no conflicts of interest.

References

1. Datiles M. Coriandrum sativum (coriander). CABI Compendium. 2022.
2. Mahleyuddin NN, Moshawih S, Ming LC, Zulkifly HH, Kifli N, Loy MJ, et al. Coriandrum sativum L.: A review on ethnopharmacology, phytochemistry, and cardiovascular benefits. Molecules. 2021;27(1):209.
3. Scandar S, Zadra C, Marcotullio MC. Coriander (Coriandrum sativum) polyphenols and their nutraceutical value against obesity and metabolic syndrome. Molecules. 2023;28(10):4187.
4. Salem MA, Manaa EG, Osama N, Aborehab NM, Ragab MF, Haggag YA, et al. Coriander (Coriandrum sativum L.) essential oil and oil-loaded nano-formulations as an anti-aging potentiality via TGFβ/SMAD pathway. Scientific reports. 2022;12(1):6578.
5. de Sousa DP, Damasceno ROS, Amorati R, Elshabrawy HA, de Castro RD, Bezerra DP, et al. Essential oils: Chemistry and pharmacological activities. Biomolecules. 2023;13(7):1144.
6. Goura K, Legrifi I, Kallali NS, Taoussi M, Kenfaoui J, Meddich A, et al. Beyond survival: the role of secondary metabolites in plant defense mechanisms. Journal of Crop Health. 2025;77(4):121.
7. Ghazanfari N, Mortazavi SA, Yazdi FT, Mohammadi M. Microwave-assisted hydrodistillation extraction of essential oil from coriander seeds and evaluation of their composition, antioxidant and antimicrobial activity. Heliyon. 2020;6(9).
8. Jeleń HH, Marcinkowska MA, Marek M. Determination of volatile terpenes in coriander cold pressed oil by vacuum assisted sorbent extraction (VASE). Molecules. 2021;26(4):884.
9. Scandar S, Zadra C, Lanari D, Marcotullio MC. Boosting the essential oil yield of Coriandrum sativum L. using choline chloride-based NADES: An optimized and systematic study employing response surface methodology (RSM). Industrial Crops and Products. 2024;208:117920.
10. Al-Khayri JM, Banadka A, Nandhini M, Nagella P, Al-Mssallem MQ, Alessa FM. Essential oil from Coriandrum sativum: A review on its phytochemistry and biological activity. Molecules. 2023;28(2):696.
11. Yammine J, Chihib N-E, Gharsallaoui A, Ismail A, Karam L. Advances in essential oils encapsulation: development, characterization and release mechanisms. Polymer Bulletin. 2024;81(5):3837-82.
12. Weisany W, Yousefi S, Soufiani SP, Pashang D, McClements DJ, Ghasemlou M. Mesoporous silica nanoparticles: A versatile platform for encapsulation and delivery of essential oils for food applications. Advances in Colloid and Interface Science. 2024;325:103116.
13. Chang H-T, Lin C-Y, Hsu L-S, Chang S-T. Thermal degradation of linalool-chemotype Cinnamomum osmophloeum leaf essential oil and its stabilization by microencapsulation with β-cyclodextrin. Molecules. 2021;26(2):409.
14. Sahu T, Ratre YK, Chauhan S, Bhaskar L, Nair MP, Verma HK. Nanotechnology based drug delivery system: Current strategies and emerging therapeutic potential for medical science. Journal of Drug Delivery Science and Technology. 2021;63:102487.
15. Musielak E, Feliczak-Guzik A, Nowak I. Optimization of the conditions of solid lipid nanoparticles (SLN) synthesis. Molecules. 2022;27(7):2202.
16. Cimino C, Maurel OM, Musumeci T, Bonaccorso A, Drago F, Souto EMB, et al. Essential oils: Pharmaceutical applications and encapsulation strategies into lipid-based delivery systems. Pharmaceutics. 2021;13(3):327.
17. Tabatabaeain S, Karimi E, Hashemi M. Essential oil-loaded solid lipid nanoparticles modified with chitosan-folate: evaluation of encapsulation efficiency, cytotoxic pro-apoptotic properties. Front Chem. 2022;10:904973.
18. Fincheira P, Espinoza J, Levio-Raiman M, Vera J, Tortella G, Brito AMM, et al. Formulation of essential oils-loaded solid lipid nanoparticles-based chitosan/PVA hydrogels to control the growth of Botrytis cinerea and Penicillium expansum. International journal of biological macromolecules. 2024;270:132218.
19. Meena M, Saxena S, Lal S, Kumar S, Meena S, Sharma Y, et al. Detection of adulteration in coriander seeds using essential oil profiling through GCMS and its correlation with physical quality and market price. Applied Food Research. 2025;5(2):101053.
20. Duong V-A, Nguyen T-T-L, Maeng H-J. Preparation of solid lipid nanoparticles and nanostructured lipid carriers for drug delivery and the effects of preparation parameters of solvent injection method. Molecules. 2020;25(20):4781.
21. Akanda M, Mithu MSH, Douroumis D. Solid lipid nanoparticles: An effective lipid-based

technology for cancer treatment. Journal of drug delivery science and technology. 2023;86:104709.
22. Tian H, Lu Z, Li D, Hu J. Preparation and characterization of citral-loaded solid lipid nanoparticles. Food Chemistry. 2018;248:78-85.
23. Dousti M, Sari S, Saffari M, Kelidari H, Asare-Addo K, Nokhodchi A. Loading Pistacia atlantica essential oil in solid lipid nanoparticles and its effect on apoptosis of breast cancer cell line MDA-MB-231. Pharmaceutical Development and Technology. 2022;27(1):63-71.
24. Gulcin İ, Alwasel SH. DPPH radical scavenging assay. Processes. 2023;11(8):2248.
25. Kumar V, Mathela C, Kumar M, Tewari G. Antioxidant potential of essential oils from some Himalayan Asteraceae and Lamiaceae species. Medicine in drug discovery. 2019;1:100004.
26. Khan MFA, Ur. Rehman A, Howari H, Alhodaib A, Ullah F, Mustafa Zu, et al. Hydrogel containing solid lipid nanoparticles loaded with argan oil and simvastatin: Preparation, in vitro and ex vivo assessment. Gels. 2022;8(5):277.
27. Nouioura G, El Fadili M, El Hachlafi N, Maache S, Mssillou I, A. Abuelizz H, et al. Coriandrum sativum L., essential oil as a promising source of bioactive compounds with GC/MS, antioxidant, antimicrobial activities: in vitro and in silico predictions. Frontiers in chemistry. 2024;12:1369745.
28. SM Abd El-Kareem M, A. Rabbih M, Elansary HO, A. Al-Mana F. Mass spectral fragmentation of Pelargonium graveolens essential oil using GC–MS semi-empirical calculations and biological potential. Processes. 2020;8(2):128.
29. Talebi SM, Naser A, Ghorbanpour M. Chemical composition and antimicrobial activity of the essential oils in different populations of Coriandrum sativum L.(coriander) from Iran and Iraq. Food Science & Nutrition. 2024;12(6):3872-82.
30. Wahba HE, Abd Rabbu HS, Ibrahim ME. Evaluation of essential oil isolated from dry coriander seeds and recycling of the plant waste under different storage conditions. Bulletin of the National Research Centre. 2020;44(1):192.
31. Bizzo HR, Brilhante NS, Nolvachai Y, Marriott PJ. Use and abuse of retention indices in gas chromatography. Journal of Chromatography A. 2023;1708:464376.
32. Chura SSD, Memória KAS, Lopes AT, Pelissari FM, Da Silveira JVW, Bezerra JdA, et al. Red sacaca essential oil-loaded nanostructured lipid carriers optimized by factorial design: cytotoxicity and cellular reactive oxygen species levels. Frontiers in Pharmacology. 2023;14:1176629.
33. Ramadan SE, El-Gizawy SA, Osman MA, Arafa MF. Application of design of experiment in the optimization of apixaban-loaded solid lipid nanoparticles: in vitro and in vivo evaluation. AAPS PharmSciTech. 2023;24(6):167.
34. Arneth B, Abdelmonem R, El-Nabarawi MA, Teaima MH, Rashwan KO, Soliman MA, Al-Samadi IEI. Optimized hesperidin-loaded lipid nanoparticles with tea tree oil for enhanced wound healing: formulation, characterization, and evaluation. Pharmaceuticals. 2025;18(3):290.
35. Hoseini B, Jaafari MR, Golabpour A, Momtazi-Borojeni AA, Karimi M, Eslami S. Application of ensemble machine learning approach to assess the factors affecting size and polydispersity index of liposomal nanoparticles. Scientific Reports. 2023;13(1):18012.
36. Kim ST, Lee HM, Jung JH, Kook J-W. Microfluidic synthesis of stable and uniform curcumin-loaded solid lipid nanoparticles with high encapsulation efficiency. RSC advances. 2025;15(14):10547-56.
37. Jeitler R, Glader C, Tetyczka C, Zeiringer S, Absenger-Novak M, Selmani A, et al. Investigation of cellular interactions of lipid-structured nanoparticles with oral mucosal epithelial cells. Frontiers in Molecular Biosciences. 2022;9:917921.
38. Mura P, Maestrelli F, D'Ambrosio M, Luceri C, Cirri M. Evaluation and comparison of solid lipid nanoparticles (SLNs) and nanostructured lipid carriers (NLCs) as vectors to develop hydrochlorothiazide effective and safe pediatric oral liquid formulations. Pharmaceutics. 2021;13(4):437.
39. Hernández-Esquivel R-A, Navarro-Tovar G, Zárate-Hernández E, Aguirre-Bañuelos P. Solid lipid nanoparticles (SLN): IntechOpen London, UK; 2022.
40. Vakili-Ghartavol M, Arouiee H, Golmohammadzadeh S, Naseri M. Synthesis, characterization, and in vitro antifungal activity of solid lipid nanoparticles containing Mentha× piperita L. essential oil. 2024.
41. Khalid A, Arshad MU, Imran A, Haroon Khalid S, Shah MA. Development, stabilization, and characterization of nanoemulsion of vitamin D3-enriched canola oil. Frontiers in nutrition. 2023;10:1205200.
42. Soleimani V, Shahdadi Sardou H, Delghandi PS, Sadeghi F, Garekani HA, Nokhodchi A, Abbaspour M. Preparation and Characterization of Solid Lipid Nanoparticles (SLNs) Containing Doxepin Hydrochloride To Enhance the Topical Delivery Through Rat Skin. BioNanoScience. 2026;16(2):150.
43. Thuy VN, Van TV, Dao AH, Lee B-J. Nanostructured lipid carriers and their potential applications for versatile drug delivery via oral administration. OpenNano. 2022;8:100064.
44. Xu L, Wang X, Liu Y, Yang G, Falconer RJ, Zhao C-X. Lipid nanoparticles for drug delivery. Advanced NanoBiomed Research. 2022;2(2):2100109.
45. Rao H, Ahmad S, Madni A, Rao I, Ghazwani M, Hani U, et al. Compritol-based

alprazolam solid lipid nanoparticles for sustained release of alprazolam: preparation by hot melt encapsulation. Molecules. 2022;27(24):8894.
46. Feng S, Sheng J, Yu J, Lin Y, Shao P. Encapsulation and release of citral using nanostructured lipid carriers: A study on the impact of different preparation methods. Food Bioscience. 2023;56:103185.
47. Noshad M, Behbahani BA, Nikfarjam Z, Zargari F. Antimicrobial activity between Coriandrum sativum seed and Cuminum cyminum essential oils against foodborne pathogens: A multi-ligand molecular docking simulation. Lwt. 2023;185:115217.
48. Kačániová M, Galovičová L, Ivanišová E, Vukovic NL, Štefániková J, Valková V, et al. Antioxidant, antimicrobial and antibiofilm activity of coriander (Coriandrum sativum L.) essential oil for its application in foods. Foods. 2020;9(3):282.
49. Amekyeh H, Billa N. Lyophilized drug-loaded solid lipid nanoparticles formulated with beeswax and theobroma oil. Molecules. 2021;26(4):908.
50. Liu L, Li L, Wan L, Mao L, Li B, Zhang X. Addition of glyceryl monostearate affects the crystallization behavior and polymorphism of palm stearin. Bioprocess and biosystems engineering. 2021;44(5):941-9.
51. Alarcon R, Walter M, Paez M, Azócar MI. Ostwald ripening and antibacterial activity of silver nanoparticles capped by anti-inflammatory ligands. Nanomaterials. 2023;13(3):428.
52. Rahman MA, Ali A, Rahamathulla M, Salam S, Hani U, Wahab S, et al. Fabrication of sustained release curcumin-loaded solid lipid nanoparticles (cur-SLNs) as a potential drug delivery system for the treatment of lung cancer: Optimization of formulation and in vitro biological evaluation. Polymers. 2023;15(3):542.
53. Chantaburanan T, Teeranachaideekul V, Jintapattanakit A, Chantasart D, Junyaprasert VB. Enhanced stability and skin permeation of ibuprofen-loaded solid lipid nanoparticles based binary solid lipid matrix: Effect of surfactant and lipid compositions. International Journal of Pharmaceutics: X. 2023;6:100205.
54. Oboh M, Elhassan E, Koorbanally NA, Govender L, Siwela M, Govender T, Mkhwanazi BN. Characterisation and In Vitro Drug Release Profiles of Oleanolic Acid-and Asiatic Acid-Loaded Solid Lipid Nanoparticles (SLNs) for Oral Administration. Pharmaceutics. 2025;17(6):723.
55. Nguyen T-T-L, Duong V-A. Solid lipid nanoparticles. Encyclopedia. 2022;2(2):952-73.
56. Veider F, Akkuş-Dağdeviren ZB, Knoll P, Bernkop-Schnürch A. Design of nanostructured lipid carriers and solid lipid nanoparticles for enhanced cellular uptake. International Journal of Pharmaceutics. 2022;624:122014.
57. Carvalho FVd, Ribeiro LNdM, Moura LDd, Rodrigues da Silva GH, Mitsutake H, Mendonça TC, et al. Docetaxel loaded in copaiba oil-nanostructured lipid carriers as a promising DDS for breast cancer treatment. Molecules. 2022;27(24):8838.
58. Yu Y, Chen D, Lee YY, Chen N, Wang Y, Qiu C. Physicochemical and in vitro digestion properties of curcumin-loaded solid lipid nanoparticles with different solid lipids and emulsifiers. Foods. 2023;12(10):2045.
59. Jamous YF, Altwaijry NA, Saleem MT, Alrayes AF, Albishi SM, Almeshari MA. Formulation and characterization of solid lipid nanoparticles loaded with troxerutin. Processes. 2023;11(10):3039.
60. Salminen H, Helgason T, Aulbach S, Kristinsson B, Kristbergsson K, Weiss J. Influence of co-surfactants on crystallization and stability of solid lipid nanoparticles. Journal of colloid and interface science. 2014;426:256-63.